

Arrangements among the Fluorophores in the Salts of Imidazole Tethered Anthracene Derivative  
with Pyridinedicarboxylic Acids Influencing Photoluminescence

**Supporting information**

Table 1S: Hydrogen bond parameters of the salts and ionic cocrystals.

Figure 1S:  $^1\text{H}$ -NMR (600 MHz, DMSO-d<sub>6</sub>) spectra of the  $\mathbf{2}[(\text{H}_3\text{anthraimida})]^{2+}[(26\text{pdc})^2 \cdot \mathbf{2}(\text{H}_2\text{26pdc})] \cdot (\text{H}_2\text{26pdc}) \cdot \text{CH}_3\text{OH}$  (**1**).

Figure 2S:  $^{13}\text{C}$ -NMR (125 MHz, DMSO-d<sub>6</sub>) spectra of the  $\mathbf{2}[(\text{H}_3\text{anthraimida})]^{2+}[(26\text{pdc})^2 \cdot \mathbf{2}(\text{H}_2\text{26pdc})] \cdot (\text{H}_2\text{26pdc}) \cdot \text{CH}_3\text{OH}$  (**1**).

Figure 3S:  $^1\text{H}$ -NMR (600 MHz, DMSO-d<sub>6</sub>) spectra of the  $(\text{H}_3\text{anthraimida})^{2+}(35\text{pdc})^2 \cdot 4\text{H}_2\text{O}$  (**2**).

Figure 4S:  $^{13}\text{C}$ -NMR (125 MHz, DMSO-d<sub>6</sub>) spectra of the  $(\text{H}_3\text{anthraimida})^{2+}(35\text{pdc})^2 \cdot 4\text{H}_2\text{O}$  (**2**).

Figure 5S:  $^1\text{H}$ -NMR (600 MHz, DMSO-d<sub>6</sub>) spectra of the  $[(\text{H}_3\text{anthraimida})]^{2+}[(26\text{pdc})]^2 \cdot \text{resorc} \cdot \text{CH}_3\text{OH} \cdot \text{H}_2\text{O}$  (**3**).

Figure 6S:  $^{13}\text{C}$ -NMR (125 MHz, DMSO-d<sub>6</sub>) spectra of the  $[(\text{H}_3\text{anthraimida})]^{2+}[(26\text{pdc})]^2 \cdot \text{resorc} \cdot \text{CH}_3\text{OH} \cdot \text{H}_2\text{O}$  (**3**).

Figure 7S:  $^1\text{H}$ -NMR (600 MHz, DMSO-d<sub>6</sub>) spectra of the  $\mathbf{2}[(\text{H}_3\text{anthraimida})]^+[(35\text{pdc})]^2 \cdot \mathbf{2}\text{resorc}$  (**4**).

Figure 8S:  $^{13}\text{C}$ -NMR (125 MHz, DMSO-d<sub>6</sub>) spectra of the  $\mathbf{2}[(\text{H}_3\text{anthraimida})]^+[(35\text{pdc})]^2 \cdot \mathbf{2}\text{resorc}$  (**4**).

Figure 9S: Powder X-ray diffraction patterns of the (a)  $\mathbf{2}[(\text{H}_3\text{anthraimida})]^{2+}[(26\text{pdc})^2 \cdot \mathbf{2}(\text{H}_2\text{26pdc})] \cdot (\text{H}_2\text{26pdc}) \cdot \text{CH}_3\text{OH}$ , (b)  $[(\text{H}_3\text{anthraimida})]^{2+}[(26\text{pdc})]^2 \cdot \text{resorc} \cdot (\text{H}_2\text{26pdc}) \cdot \text{CH}_3\text{OH}$ , (c)  $(\text{H}_3\text{anthraimida})^{2+}(35\text{pdc})^2 \cdot 4\text{H}_2\text{O}$ , (d)  $\mathbf{2}[(\text{H}_2\text{anthraimida})]^+[(35\text{pdc})]^2 \cdot \mathbf{2}\text{resorc}$  (Red = Experimental, Black = Simulated). Simulated pattern generated from CIF file).

Figure 10S: Scanning electron microscope images of (a)  $\mathbf{2}[(\text{H}_3\text{anthraimida})]^{2+}[(26\text{pdc})^2 \cdot \mathbf{2}(\text{H}_2\text{26pdc})] \cdot (\text{H}_2\text{26pdc}) \cdot \text{CH}_3\text{OH}$ , (b)  $(\text{H}_3\text{anthraimida})^{2+}(35\text{pdc})^2 \cdot 4\text{H}_2\text{O}$  (c)  $[(\text{H}_3\text{anthraimida})]^{2+}[(26\text{pdc})]^2 \cdot \text{resorc} \cdot \text{CH}_3\text{OH} \cdot \text{H}_2\text{O}$ , (d)  $\mathbf{2}[(\text{H}_2\text{anthraimida})]^+[(35\text{pdc})]^2 \cdot \mathbf{2}\text{resorc}$ .

Figure 11S: Thermogravimetry of the  $(\text{H}_3\text{anthraimida})^{2+}(35\text{pdc})^2 \cdot 4\text{H}_2\text{O}$  (**2**) (heating rate 10°C /minute)

Figure 12S: The pH titrations of **Hanthraimida** (4mL, 1mM in methanol) (i) with hydrochloric acid(1 mM) (ii) with **H<sub>2</sub>26pdc** (1mM in methanol) (iii) with **H<sub>2</sub>35pdc** and (iv) and (iv) are same titrations as (ii) and (iii) but each solution contained 1mM **Hanthraimida** with 1 mM resorcinol.

Figure 13S: Fluorescence titration (excitation at 365 nm) of **Hanthraimida** ( $10^{-5}$  M in ethanol) with **H<sub>2</sub>35pdc** (10  $\mu$ l aliquot of  $10^{-5}$  M in Ethanol).

Figure 14S: The changes in the normalized fluorescence intensities at 418 nm of **Hanthraimida** ( $10^{-5}$  M) at different concentrations of pyridine dicarboxylic acids.

Figure 15S: Time resolved fluorescence emission of solid sample of **1** ( $\lambda_{\text{ex}} = 405$  nm;  $\lambda_{\text{em}}, 490$  nm).

Figure 16S: Time resolved fluorescence emission of solid sample of **2** ( $\lambda_{\text{ex}}, 405$  nm;  $\lambda_{\text{em}}, 490$  nm).

Figure 17S: Time resolved fluorescence emission of solid sample of **3** ( $\lambda_{\text{ex}}, 405$  nm;  $\lambda_{\text{em}}, 480$  nm).

Figure 18S: Time resolved fluorescence emission of solid sample of **4** ( $\lambda_{\text{ex}}$ , 405 nm;  $\lambda_{\text{em}}$ , 480 nm).  
 Figure 19S: Emission spectra of the solid sample of **1** upon irradiation at different wavelengths  
 Figure 20S: Emission spectra of the solid sample of **2** upon irradiation at different wavelengths.  
 Figure 21S: Emission and excitation spectra of the solid sample of **1** upon irradiation by wavelength = 325nm.  
 Figure 22S: Emission and excitation spectra of the solid sample of **2** upon irradiation by wavelength = 325nm.  
 Figure 23S: Emission and excitation spectra of the solid sample of **3** upon irradiation by wavelength = 325nm.  
 Figure 24S: Emission and excitation spectra of the solid sample of **4** upon irradiation by wavelength = 325nm.  
 Figure 25S: The visual colour of the solid samples of **1-4** under UV-lamp.  
 Figure 26S: Solid-state photoluminescence of the compound **2** at different slit width (band pass black = 5 nm, red = 4 nm and Blue = 2 nm) upon irradiation by wavelength = 325nm. (Recorded on a HORIBA FLUOROMAX-4P; Serial No. 0644D-2510-FM).  
 Figure 27S: Solid-state photoluminescence of the compound **3** at different slit width (band pass black = 5 nm, red = 4 nm and Blue = 2 nm) upon irradiation by wavelength = 325nm. (Recorded on a HORIBA FLUOROMAX-4P; Serial No. 0644D-2510-FM).  
 Figure 28S: UV-vis spectra of the cocrystals **1**, **2**, **3**, **4** and **Hanthraimida** ( $10^{-6}$  M in DMSO).  
 Figure 29S: Thermogravimetry of the cocrystal **1** (heating rate 10°C /minute)/  
 Figure 30S: Thermogravimetry of the cocrystal **3** (heating rate 10°C /minute)/  
 Figure 31S: Thermogravimetry of the cocrystal **4** (heating rate 10°C /minute).  
 Figure 32S: Solid state UV-visible spectra of the cocrystals **1-4**.

### Spectroscopic data of the salts and cocrystals:

**2[(H<sub>3</sub>anthraimida)]<sup>2+</sup>[(26pdc)<sup>2-</sup>·2(H<sub>2</sub>26pdc)<sup>-</sup>]·(H<sub>2</sub>26pdc)·CH<sub>3</sub>OH (1):** Isolated yield: 71 % <sup>1</sup>H-NMR (600 MHz, DMSO- *d*<sub>6</sub>, ppm): 8.73 (s, 1H), 8.43 (d, *J* = 6 Hz, 2H), 8.15 (d, *J* = 6 Hz, 2H), 8.13 (s, 4H), 8.08 (t, *J* = 12 Hz, 2H), 7.73 (s, 1H), 7.64 (t, *J* = 6 Hz, 2H), 7.58 (t, *J* = 6 Hz, 2H), 7.18 (s, 1H), 6.95 (s, 1H), 5.15 (s, 2H), 4.10 (t, *J* = 6 Hz, 2H), 3.20-3.17 (m, 5H), 2.15 (p, *J* = 6 Hz, 2H). <sup>13</sup>C NMR (125 MHz, DMSO-*d*<sub>6</sub>, ppm): 171.1, 151.4, 150.2, 142.3, 142.2, 136.1, 135.8, 134.9, 134.3, 132.6, 132.3, 132.0, 130.8, 129.6, 124.9, 50.65, 48.9, 47.9, 32.5. IR (Neat, cm<sup>-1</sup>): 3480 (m), 3049 (m), 2828 (m), 1710 (m), 1563 (m), 1450 (w), 1414 (w), 1369 (w), 1309 (w), 1158 (w), 1105 (w), 1074 (w), 993 (w), 873 (w), 815 (w), 756 (m), 731 (s), 690 (s), 645 (s), 558 (w), 460 (w), 415 (m). Melting point 216.2 °C

**(H<sub>3</sub>anthraimida)<sup>2+</sup>(35pdc)<sup>2-</sup>·4H<sub>2</sub>O (2):** Isolated yield: 73 % <sup>1</sup>H NMR (600 MHz, DMSO-*d*<sub>6</sub>, ppm) : 9.12 (s, 2H), 8.70 (s, 1H), 8.61 (s, 1H), 8.49 (d, *J* = 6 Hz, 2H), 8.15 (d, *J* = 6 Hz, 2H),

7.66 (s, 1H), 7.62 (t,  $J$  = 6 Hz, 2H), 7.56 (t,  $J$  = 6 Hz, 2H), 7.17 (s, 1H), 6.91 (s, 1H), 5.04 (s, 2H), 4.09 (t,  $J$  = 6 Hz, 2H), 3.06 (t,  $J$  = 6 Hz, 2H), 2.12 (p,  $J$  = 6 Hz, 2H).  $^{13}\text{C}$  NMR (125 MHz, DMSO-d<sub>6</sub>, ppm): 166.9, 153.0, 137.6, 137.6, 135.1, 131.1, 130.9, 129.4, 129.0, 128.6, 127.3, 127.0, 125.8, 125.0, 119.9, 46.1, 44.1, 43.7, 29.0. IR (Neat, cm<sup>-1</sup>): 3620 (w), 3280 (br, w), 3147 (w), 1626 (s), 1546 (m), 1350 (s), 1288 (w), 1107 (m), 1026 (m), 813 (m), 769 (m), 746 (w), 723 (s), 660 (w), 634 (m), 601 (m), 573 (m), 502 (w), 424 (m). Melting point 232.4 °C.

**[H<sub>3</sub>anthraimida]<sup>2+</sup>[(26pdc)]<sup>2-</sup>·resorc·CH<sub>3</sub>OH·H<sub>2</sub>O (3):** Isolated yield: 68 %  $^1\text{H}$  NMR (600 MHz, DMSO-d<sub>6</sub>, ppm) : 8.67 (s, 1H), 8.44 (d,  $J$  = 6 Hz, 2H), 8.12 (d,  $J$  = 6 Hz, 2H), 8.08 (d,  $J$  = 6 Hz, 2H), 8.03 – 8.00 (m, 1H), 7.66 (s, 1H), 7.59-7.53 (m, 4H), 7.13 (s, 1H), 6.93 – 6.90 (m, 2H), 6.20 – 6.18 (m, 3H), 5.04 (s, 2H), 4.07 (t,  $J$  = 6 Hz, 2H), 3.07 (t,  $J$  = 6 Hz, 2H), 2.11 (p,  $J$  = 6 Hz, 2H).  $^{13}\text{C}$  NMR (125 MHz, DMSO-d<sub>6</sub>, ppm): 167.0, 158.9, 150.8, 138.9, 137.6, 131.3, 130.9, 130.2, 129.4, 129.3, 128.5, 127.1, 126.3, 125.8, 124.9, 119.8, 106.7, 102.9, 49.0, 45.7, 44.0, 43.4, 28.71. IR (Neat, cm<sup>-1</sup>): 3049 (br,w), 1603 (m), 1556 (s), 1476 (m), 1449 (w), 1360 (s), 1167 (w), 1147 (m), 1080 (w), 993 (w), 962 (m), 852 (m), 733 (s), 713 (m), 648 (m), 631 (m), 601 (w), 539 (w), 459 (w), 417 (m). Melting point 181.5 °C

**2[(H<sub>2</sub>anthraimida)]<sup>+</sup>[(35pdc)]<sup>2-</sup>·2resorc (4):** Isolated yield: 66 %  $^1\text{H}$  NMR (600 MHz, DMSO-d<sub>6</sub>, ppm) : 9.08 (s, 2H), 8.63 (s, 2H), 8.59 (t,  $J$  = 2.0 Hz, 1H), 8.45 (d,  $J$  = 12 Hz, 4H), 8.12 (d,  $J$  = 6 Hz, 4H), 7.62 – 7.59 (m, 6H), 7.56 – 7.54 (t,  $J$  = 6 Hz, 4H), 7.12 (s, 2H), 6.93-6.90 (m, 2H), 6.88 (s, 2H), 6.19-6.18 (m, 6H), 4.84 (s, 4H), 4.05 (t,  $J$  = 6 Hz, 4H), 2.90 (t,  $J$  = 6 Hz, 4H), 2.01 (p,  $J$  = 6 Hz, 4H).  $^{13}\text{C}$  NMR (125 MHz, DMSO-d<sub>6</sub>, ppm): 166.9, 158.9, 152.7, 137.6, 137.5, 131.5, 130.7, 130.2, 129.4, 128.7, 128.2, 126.8, 125.7, 125.0, 119.8, 106.7, 102.9, 46.5, 44.6, 44.3, 40.4, 30.1. IR (Neat, cm<sup>-1</sup>): 3053 (br, w), 1600 (m), 1513 (w), 1474 (m), 1448 (w), 1432 (m), 1363 (s), 1307 (w), 1283 (w), 1225 (w), 1168 (m), 1146 (m), 1110 (m), 1085 (m), 1050 (w), 1030 (w), 962 (m), 926 (w), 895 (w), 842 (m), 811 (m), 785 (w), 768 (m), 730 (s), 691 (w), 683 (w), 656 (w), 629 (w), 601 (w), 539 (w), 502 (w), 458 (w), 415 (m). Melting point 143.1 °C.

**Melting point of Hanthraimida-** 130-132 °C

**Table 1S:** Hydrogen bond parameters of the salts and ionic cocrystals.

Salts	D-H···A	d <sub>D-H</sub> (Å)	d <sub>H···A</sub> (Å)	d <sub>D···A</sub> (Å)	∠D-H···A (°)
-------	---------	----------------------	------------------------	------------------------	--------------



<b>2[(H<sub>3</sub>anthraimida)]<sup>+</sup>[(35pdc)]<sup>2-</sup></b>	N(3) -H(3N')...O(2) [x,y,z]	0.89	1.90	2.729(3)	154
<b>·2resorc</b>	N(7) -H(7N')...O(4) [1-x,1-y,-z]	0.89	1.88	2.694(3)	152
	N(3) -H(3N)...O(1) [1-x,1-y,1-z]	0.89	1.94	2.742(3)	148
	O(5) -H(5O)...O(2) [x,y,z]	1.03(6)	1.91(6)	2.769(4)	140(6)
	O(6) -H(6O)...N(4) [x,-1+y,z]	0.82	1.98	2.739(4)	154
	N(7) -H(7N)...O(3) [x,y,z]	0.89	1.89	2.698(4)	150
	O(7) -H(7O)...N(1) [1-x,-y,1-z]	0.82	1.92	2.734(4)	169
	O(8) -H(8O)...N(5) [1-x,-y,-z]	0.82	1.90	2.708(4)	169
	C(6) -H(6B)...O(5) [x,y,z]	0.97	2.52	3.384(4)	148
	C(42) -H(42)...O(4) [x,-1+y,z]	0.93	2.55	3.471(5)	169

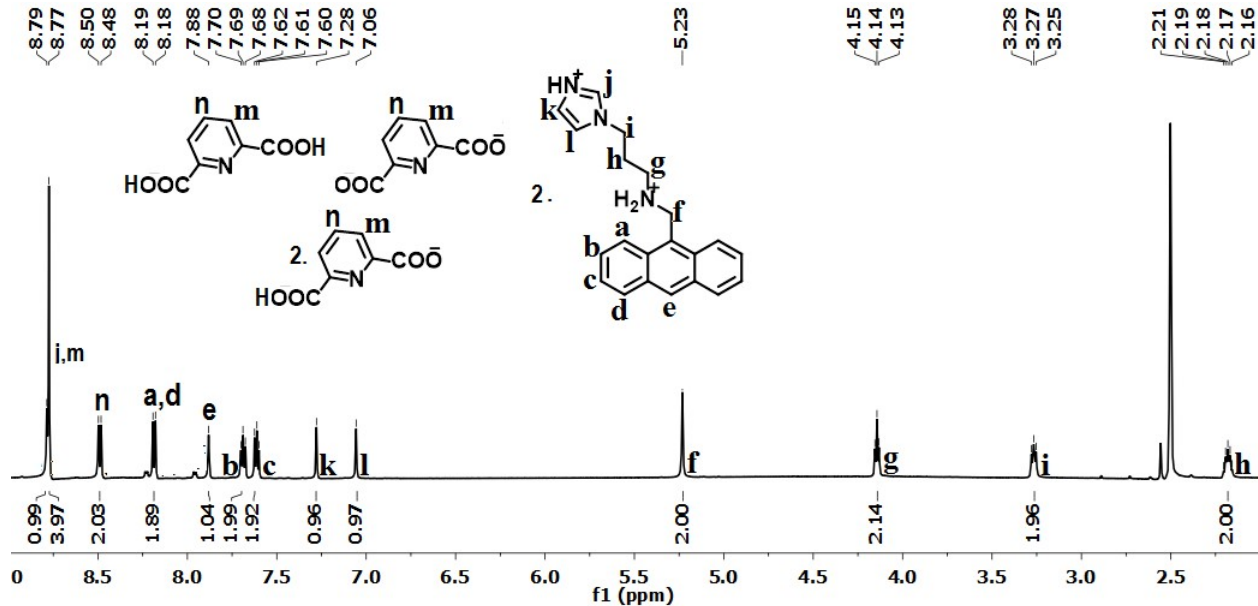


Figure 1S: <sup>1</sup>H-NMR (600 MHz, DMSO-d<sub>6</sub>) spectra of the **2[(H<sub>3</sub>anthraimida)]<sup>2+</sup>[(26pdc)<sup>2-</sup>]  
·2(H<sub>2</sub>6pdc)<sup>-</sup>·(H<sub>2</sub>26pdc)·CH<sub>3</sub>OH (1).**

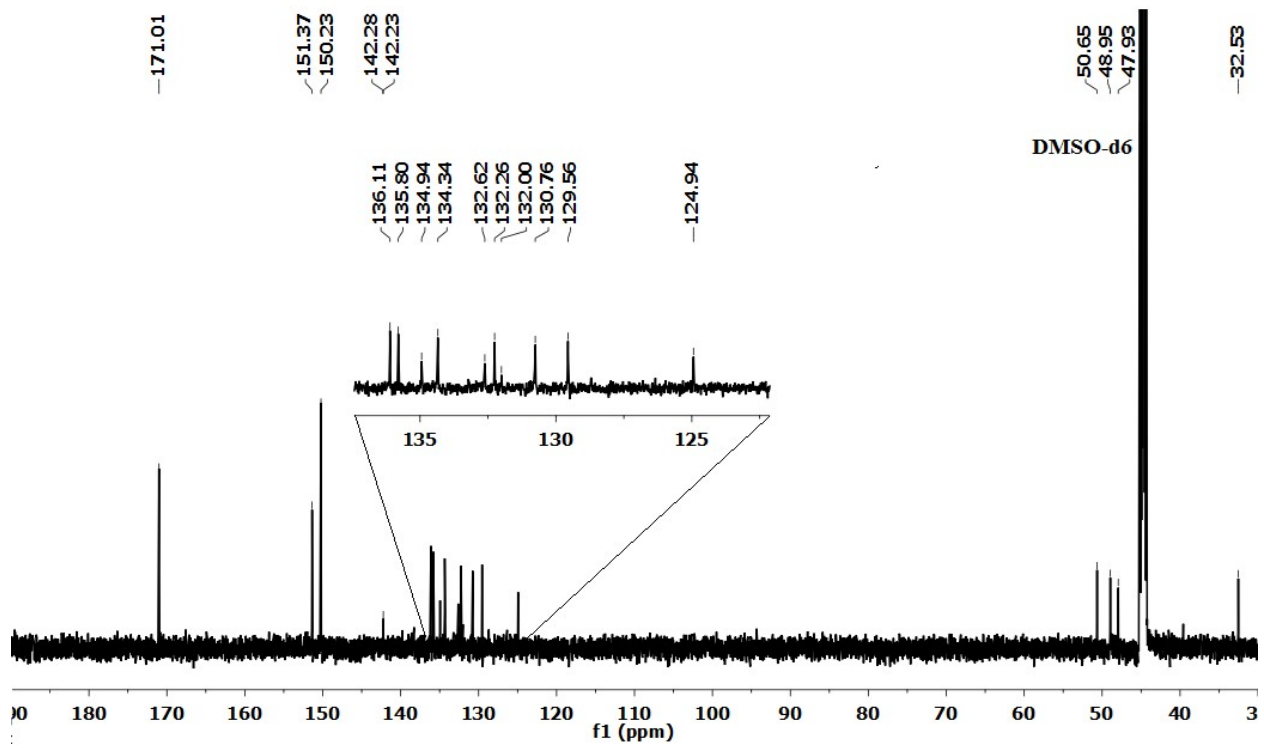


Figure 2S:  $^{13}\text{C}$ -NMR (125 MHz, DMSO-d<sub>6</sub>) spectra of the  $2[(\text{H}_3\text{anthraimida})]^{2+}[(26\text{pdc})^{2-} \cdot 2(\text{H}_2\text{26pdc}) \cdot (\text{H}_2\text{26pdc}) \cdot \text{CH}_3\text{OH}$  (1).

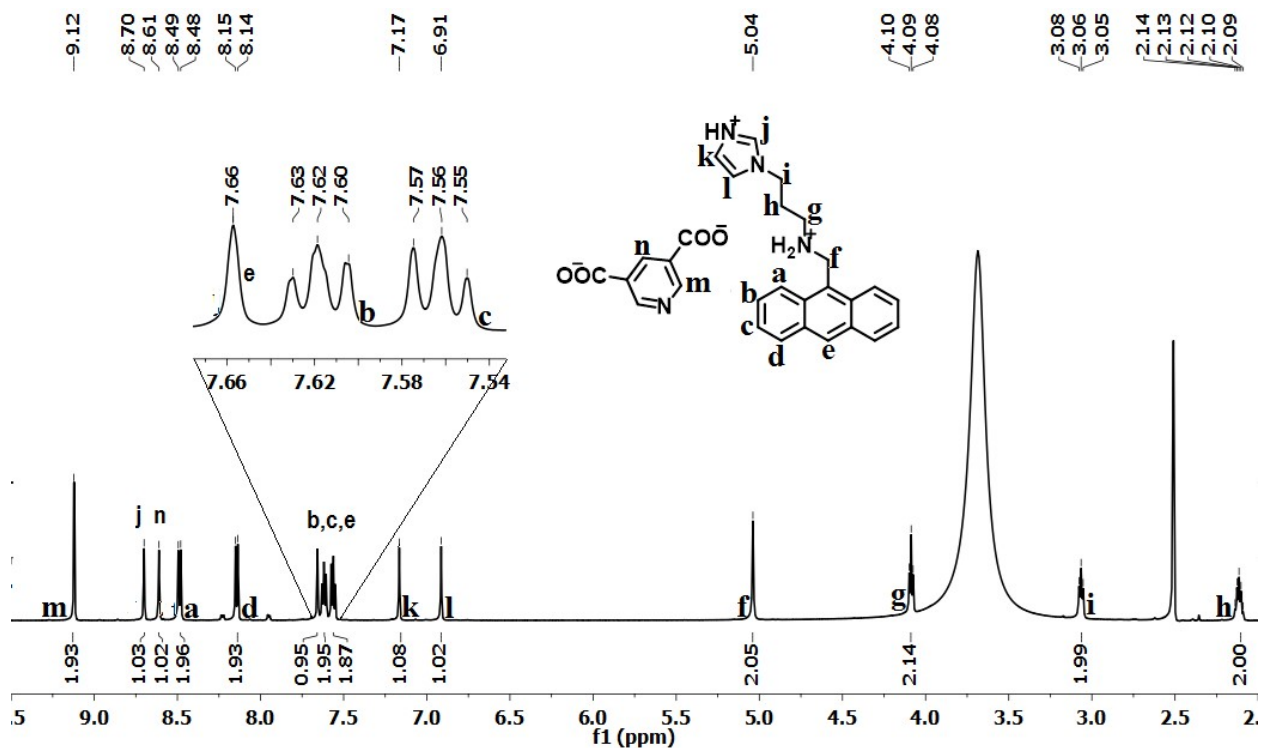


Figure 3S:  $^1\text{H}$ -NMR (600 MHz,  $\text{DMSO-d}_6$ ) spectra of the  $(\text{H}_3\text{anthraimida})^{2+}(35\text{pdc})^{2-}\cdot 4\text{H}_2\text{O}$  (2).

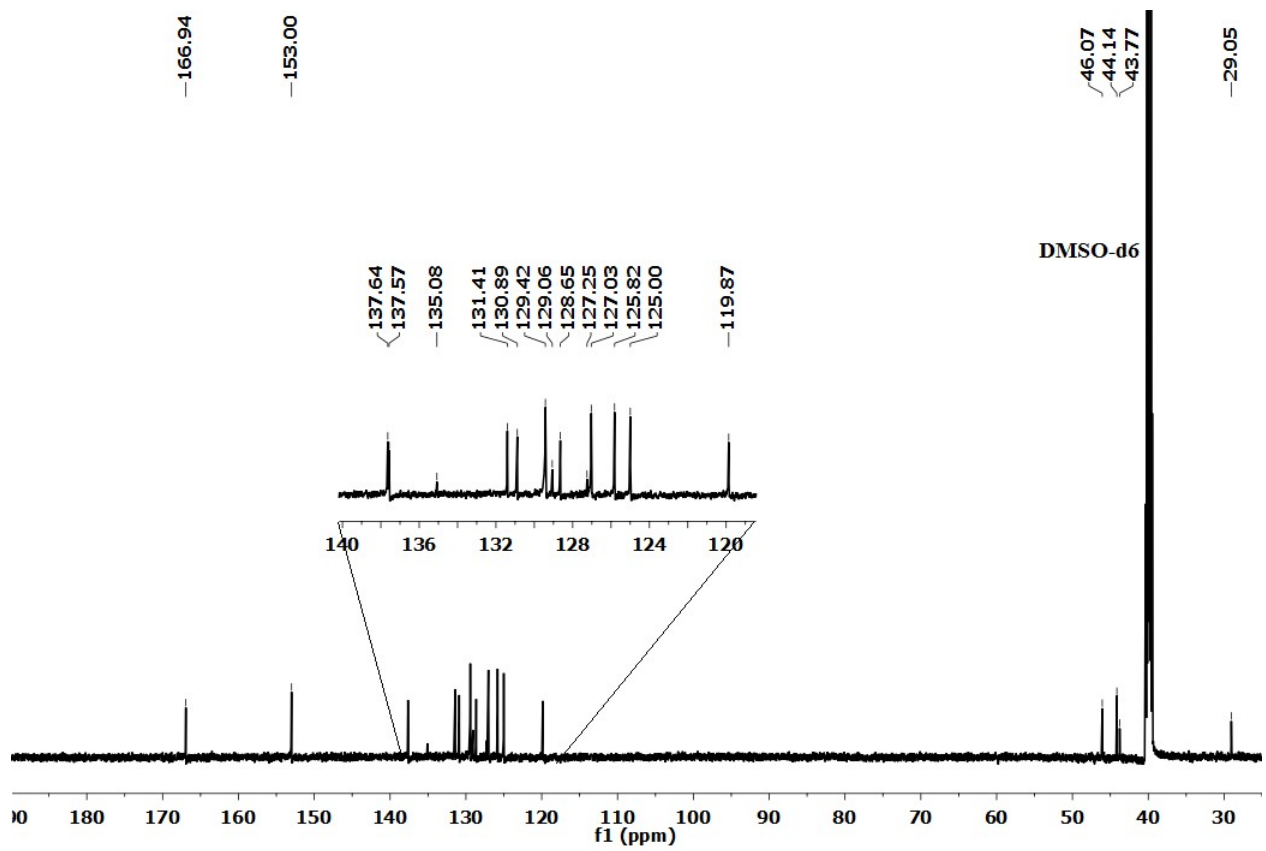


Figure 4S: <sup>13</sup>C-NMR (125 MHz, DMSO-d<sub>6</sub>) spectra of (H<sub>3</sub>anthraimida)<sup>2+</sup>(35pdc)<sup>2-</sup>·4H<sub>2</sub>O (2).

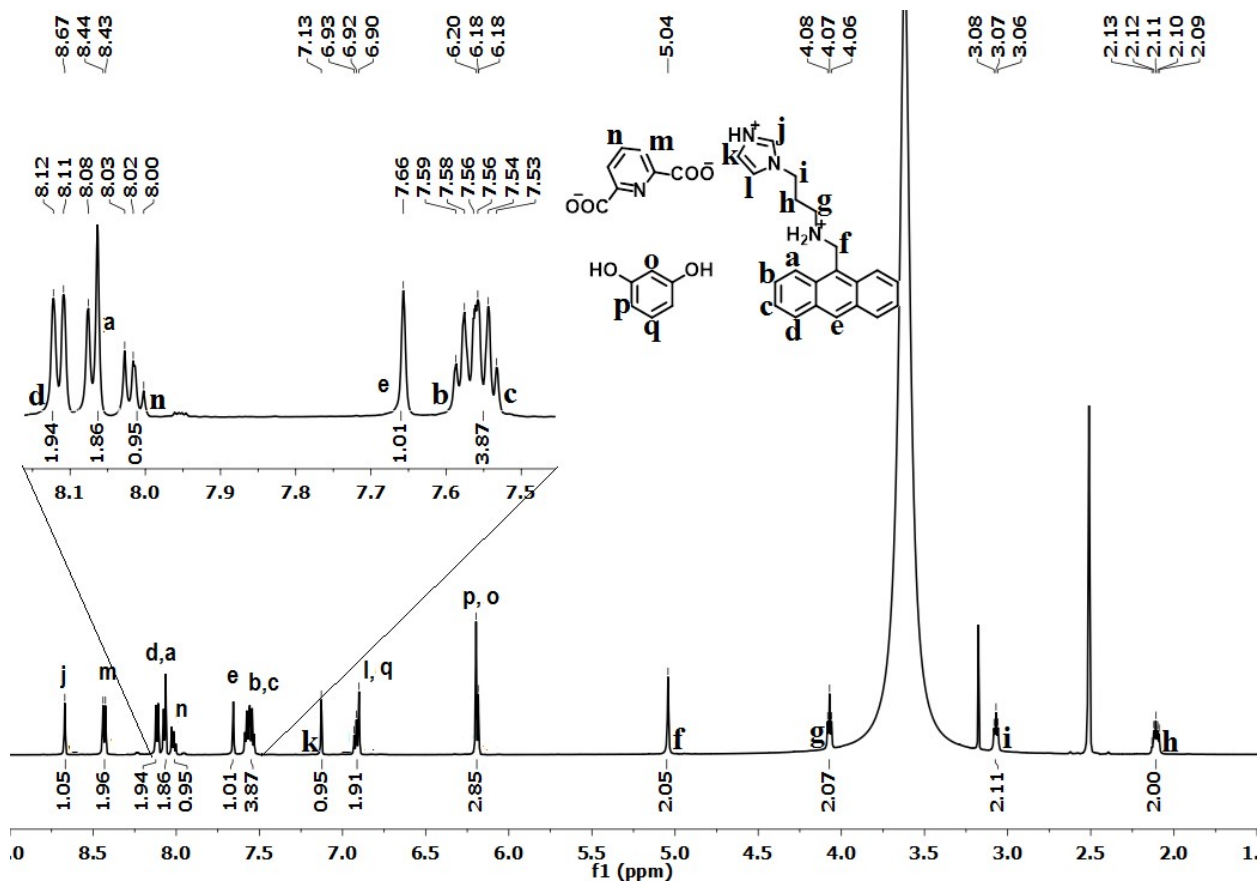


Figure 5S:  $^1\text{H-NMR}$  (600 MHz, DMSO- $\text{d}_6$ ) spectra of the  $[(\text{H}_3\text{anthraimida})]^{2+}[(26\text{pdc})]^{2-}\cdot\text{resorc}\cdot\text{CH}_3\text{OH}\cdot\text{H}_2\text{O}$  (3).

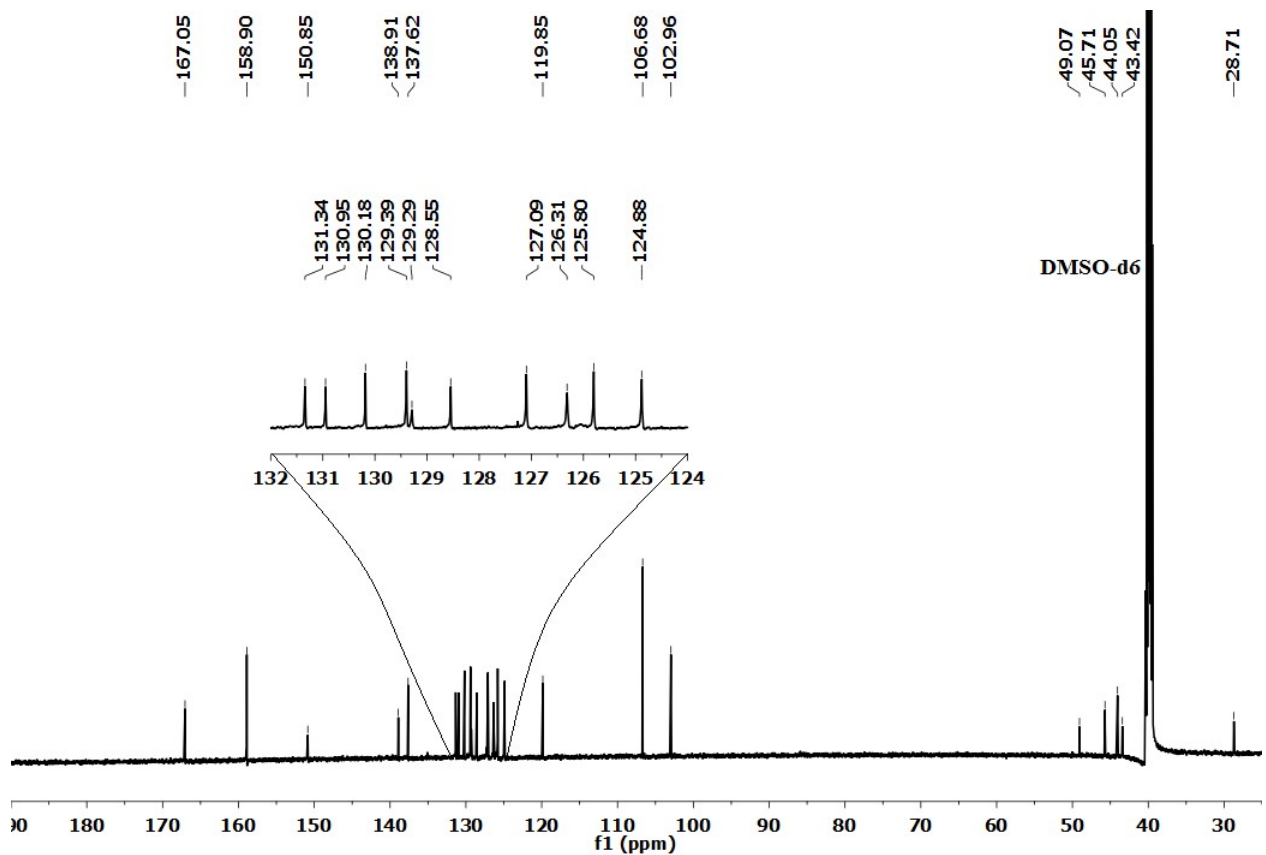


Figure 6S:  $^{13}\text{C}$ -NMR (125 MHz, DMSO-d<sub>6</sub>) spectra of the  $[(\text{H}_3\text{anthraimida})]^{2+}[(26\text{pdc})]^{2-} \cdot \text{resorc}\cdot\text{CH}_3\text{OH}\cdot\text{H}_2\text{O}$  (**3**).

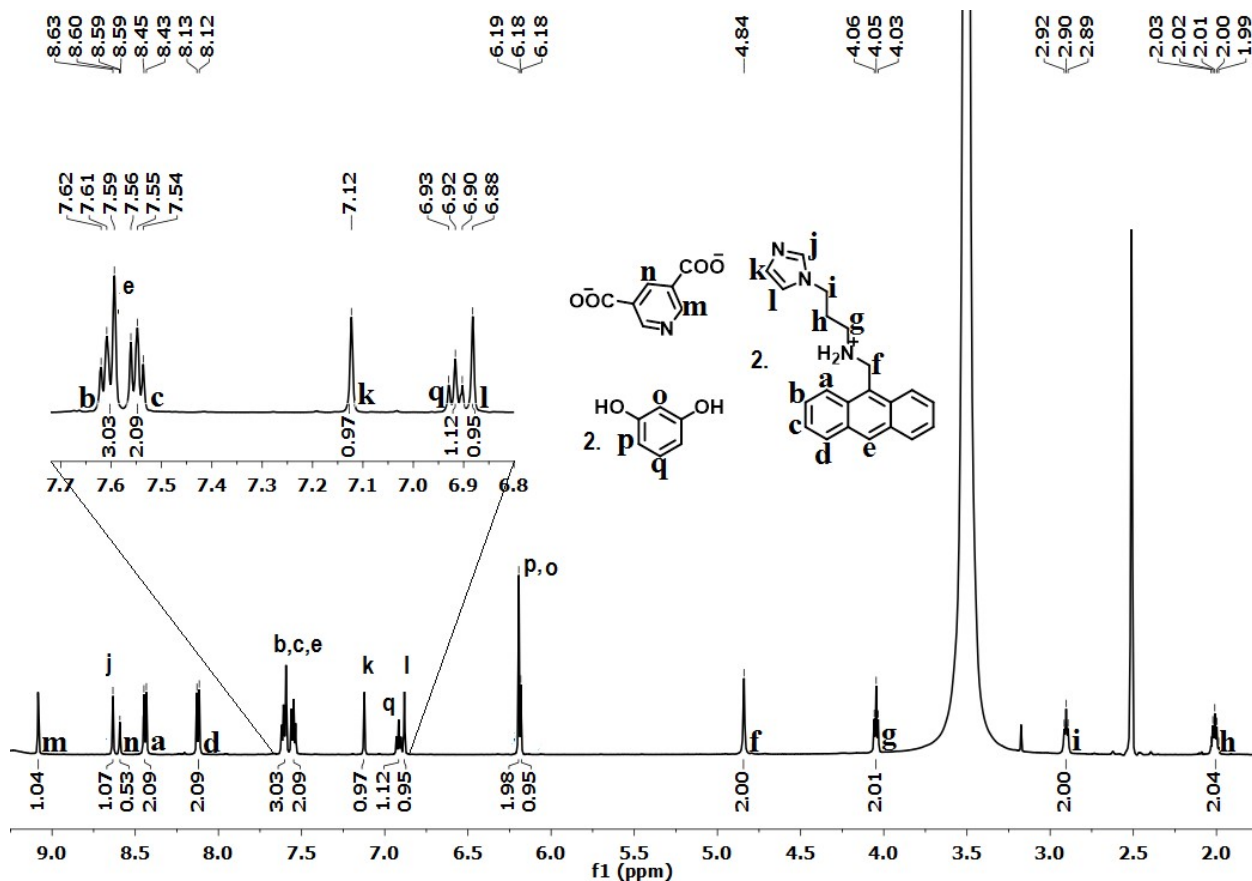


Figure 7S:  $^1\text{H-NMR}$  (600 MHz, DMSO- $\text{d}_6$ ) spectra of the **2** $[(\text{H}_2\text{anthraimida})]^+[(35\text{pdc})]^{2-}\cdot\text{2resorc} (**4**).$

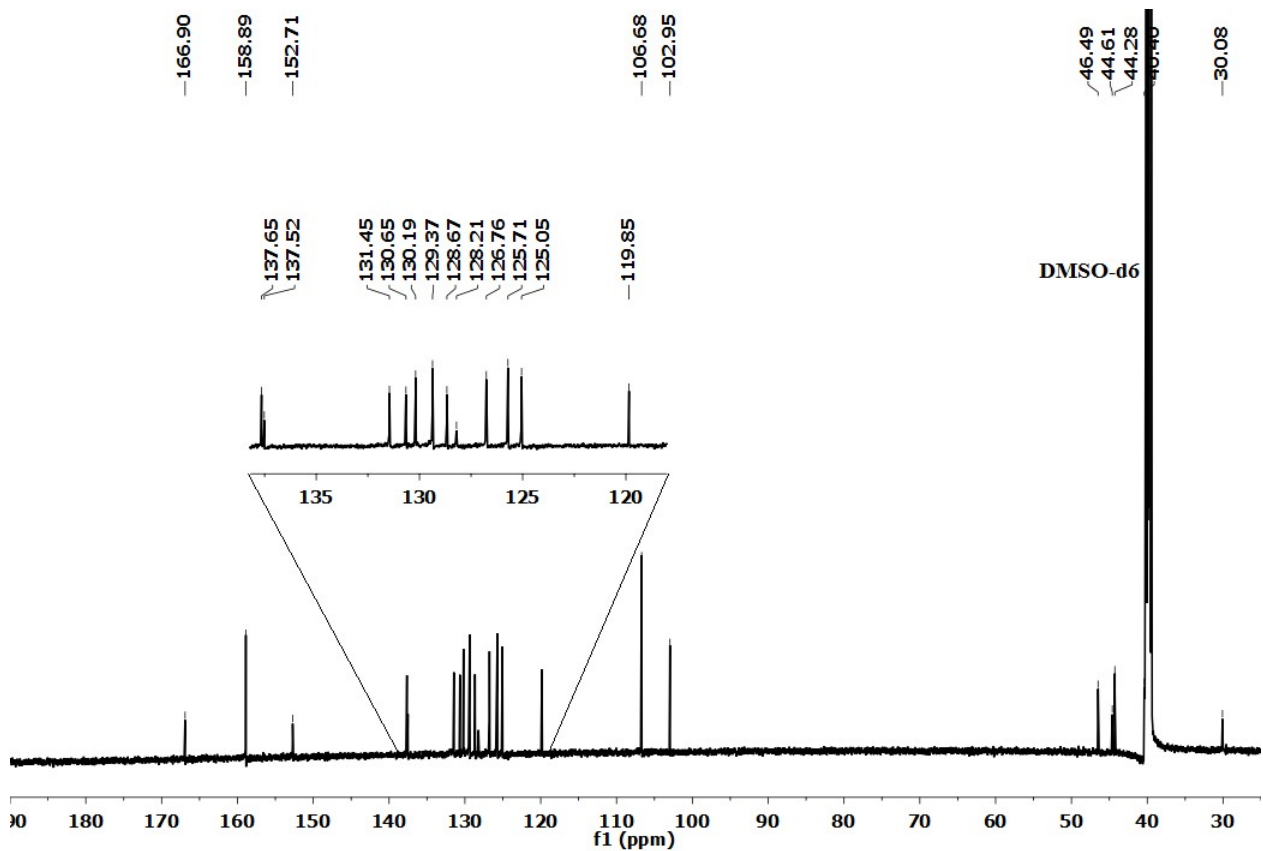


Figure 8S:  $^{13}\text{C}$ -NMR (125 MHz, DMSO- $\text{d}_6$ ) spectra of the **2** $[(\text{H}_2\text{anthraimida})]^+[(35\text{pdc})]^2$   
**·2resorc** (**4**).

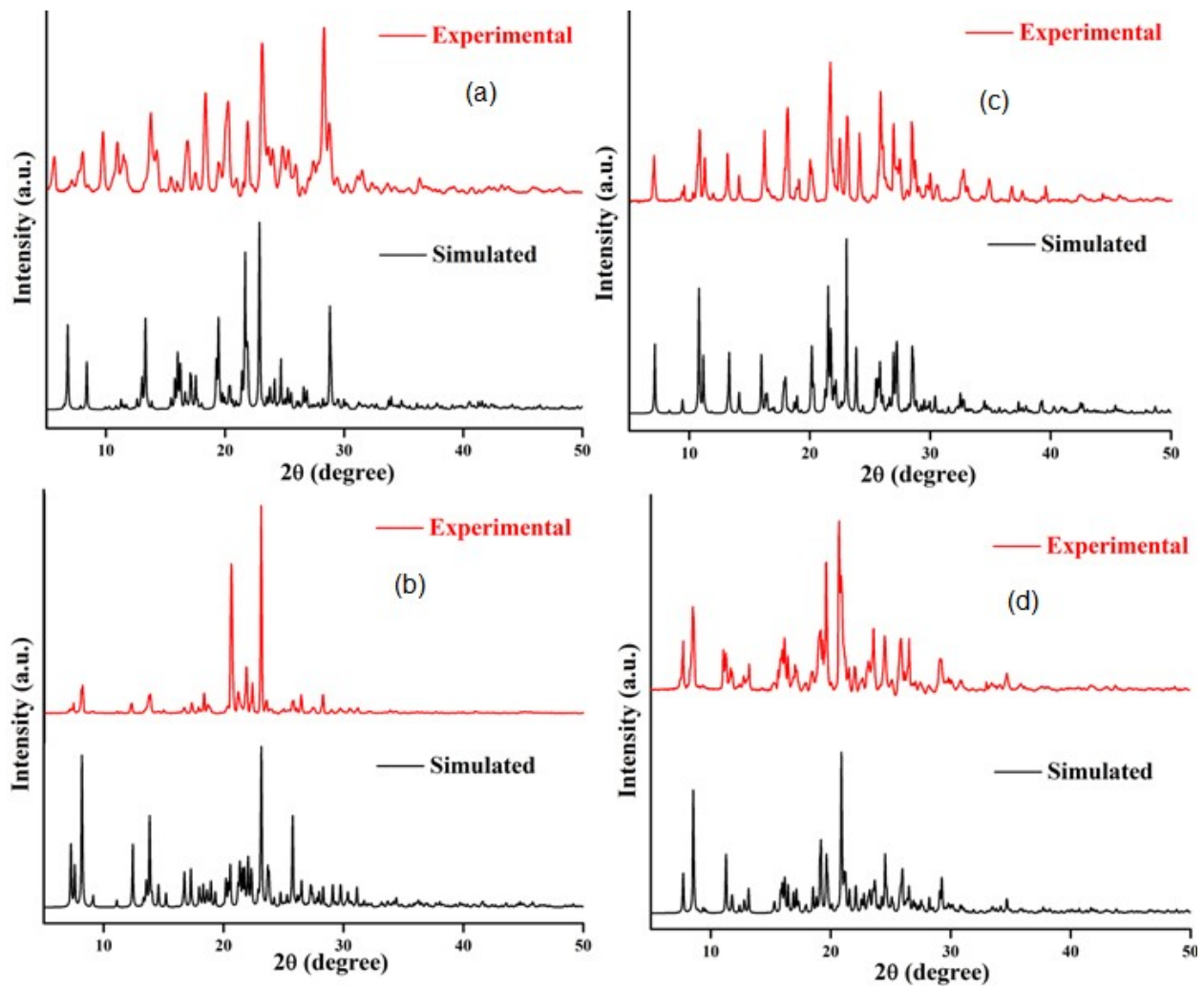


Figure 9S: Powder X-ray diffraction patterns of the (a)  $2[(H_3\text{anthraimida})]^{2+}[(26\text{pdc})^{2-}\cdot 2(\text{H}_2\text{26pdc})]\cdot(\text{H}_2\text{26pdc})\cdot\text{CH}_3\text{OH}$ , (b)  $[(H_3\text{anthraimida})]^{2+}[(26\text{pdc})]^{2-}\cdot\text{resorc}\cdot(\text{H}_2\text{26pdc})\cdot\text{CH}_3\text{OH}$ , (c)  $(H_3\text{anthraimida})^{2+}(35\text{pdc})^{2-}\cdot 4\text{H}_2\text{O}$ , (d)  $2[(H_3\text{anthraimida})]^+[(35\text{pdc})]^{2-}\cdot 2\text{resorc}$  (Red = Experimental, Black = Simulated). Simulated pattern generated from CIF file).

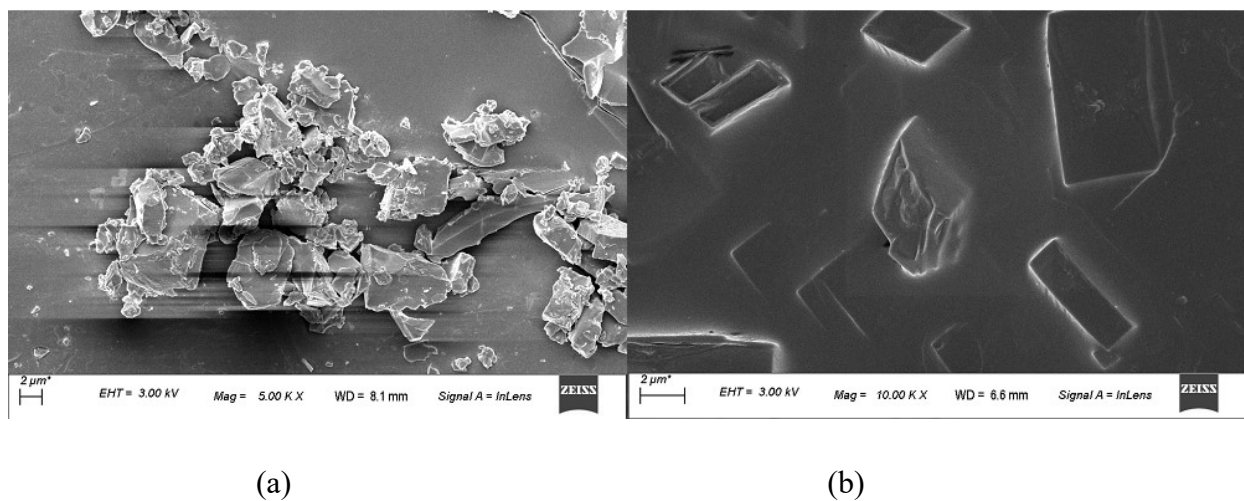


Figure 10S: Scanning electron microscope images of (a)  $[(\text{H}_3\text{anthraimida})]^{2+}[(26\text{pdc})]^{2-}\cdot\text{resorc}\cdot\text{CH}_3\text{OH}\cdot\text{H}_2\text{O}$ , (b)  $2[(\text{H}_2\text{anthraimida})]^+[(35\text{pdc})]^{2-}\cdot 2\text{resorc}$ .

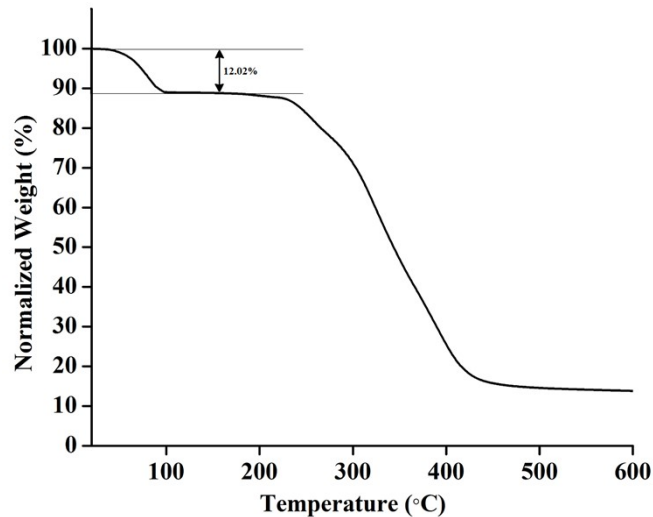


Figure 11S: Thermogravimetry of the ( $\text{H}_3\text{anthraimida}$ ) $^{2+}$ (35pdc) $^{2-}$  $\cdot$ 4H<sub>2</sub>O (**2**) (heating rate 10°C/minute). Theoretical value of loss of four water molecules is 12.98% and experimental value is 12.02%.

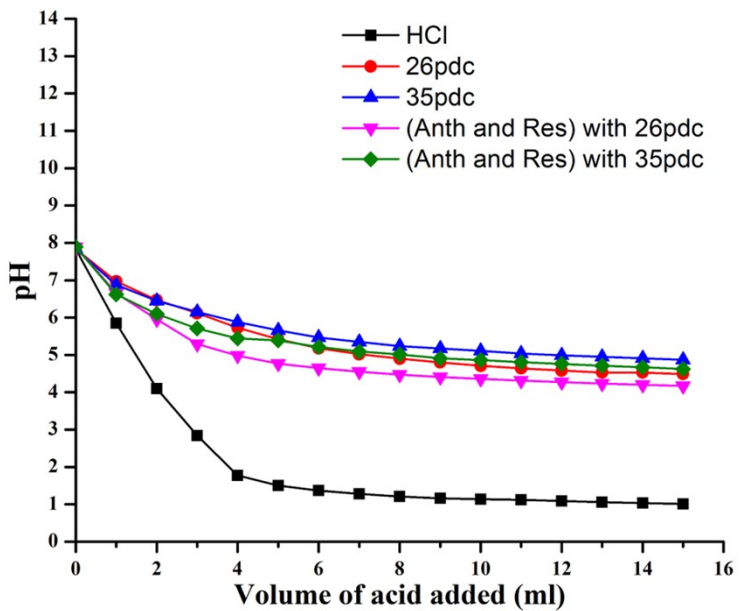


Figure 12S: The pH titrations of **Hanthraimida** (4mL, 1mM in methanol ) (i) with HCl (1 mM) (ii) with H<sub>2</sub>**26pdc** (1mM in methanol) (iii) with H<sub>2</sub>**35pdc** and (iii) and (iv) are same titrations as (ii) and (iii) but each solution contained 1mM **Hanthraimida** with 1mM resorcinol.

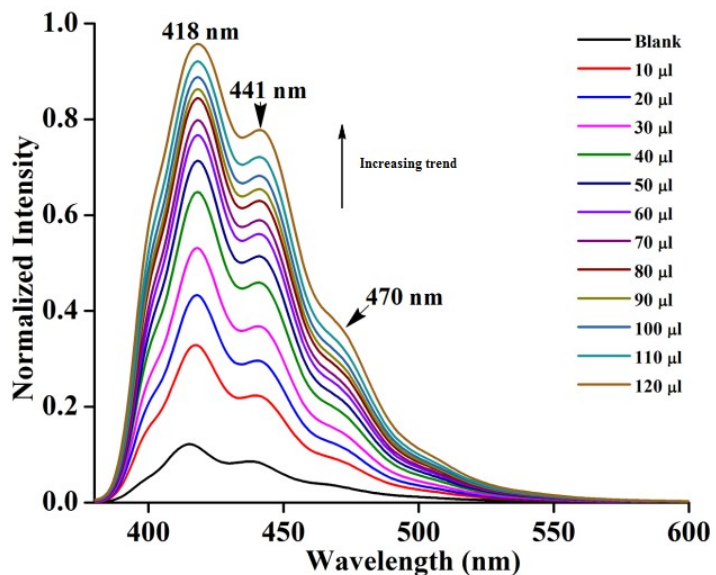


Figure 13S: Fluorescence titration (excitation at 365 nm) of **Hanthraimida** ( $10^{-5}$  M in ethanol) with H<sub>2</sub>**35pdc** (10  $\mu$ l aliquot of  $10^{-5}$  M in ethanol).

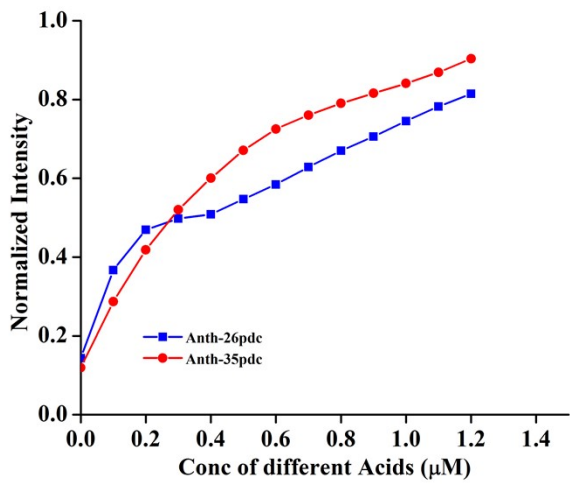
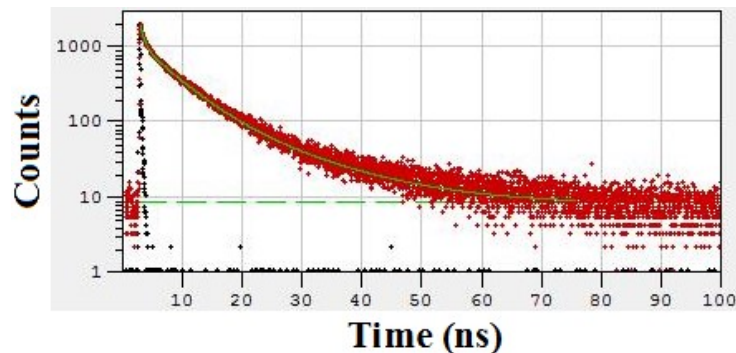


Figure 14S: The changes in the normalized fluorescence intensities at 418 nm of **Hanthraimida** ( $10^{-5}$  M) at different concentrations of pyridine dicarboxylic acids.



#### Exponential Components Analysis (Reconvolution)

Fitting range : [104; 3100] channels

$\chi^2$  : 1.089

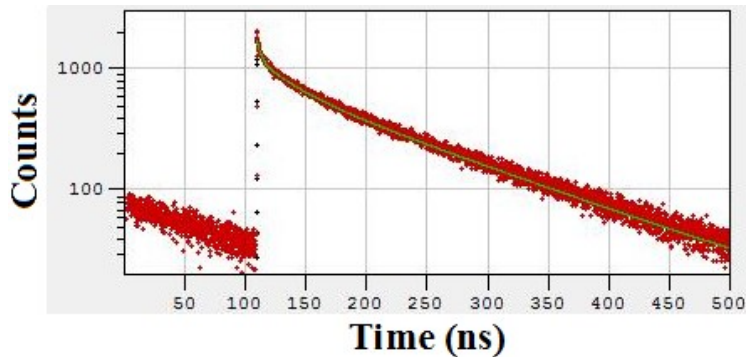
	B <sub>i</sub>	$\Delta B_i$	f <sub>i</sub> (%)	$\Delta f_i$ (%)	$\tau_i$ (ns)	$\Delta \tau_i$ (ns)
1	0.2670	0.2200	24.540	22.096	0.654	0.050
2	0.0663	0.0070	48.925	5.189	5.252	0.005
3	0.0138	0.0016	26.534	3.103	13.706	0.003

Shift : -1.001 ns ( $\pm 22.392$  ns)

Decay Background : 8.120 ( $\pm 0.298$ )

IRF background : 0.100

Figure 15S: Time resolved fluorescence emission of solid sample of **1** ( $\lambda_{ex}$ ,405 nm;  $\lambda_{em}$ ,490 nm).



#### Exponential Components Analysis (Tail Fitting)

Fitting range : [880; 4096] channels

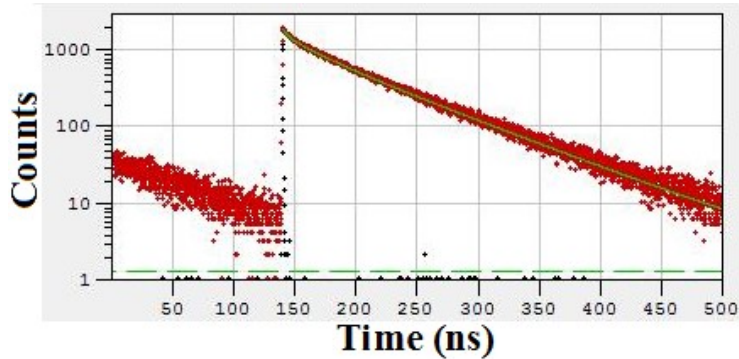
$\chi^2$  : 1.049

	B <sub>i</sub>	$\Delta B_i$	f <sub>i</sub> (%)	$\Delta f_i$ (%)	$\tau_i$ (ns)	$\Delta \tau_i$ (ns)
1	543.8052	17.3091	1.816	0.067	3.470	0.017
2	448.5926	11.2802	11.865	0.299	27.479	0.002
3	746.7656	12.5292	86.319	1.448	120.095	0.0001

Shift : 0 ns ( $\pm 0$  ns)

Decay Background : 4.797 ( $\pm 1.259$ )

Figure 16S: Time resolved fluorescence emission of solid sample of **2** ( $\lambda_{\text{ex}}$ , 405 nm;  $\lambda_{\text{em}}$ , 490 nm).



#### Exponential Components Analysis (Tail Fitting)

Fitting range : [1131; 4096] channels

$\chi^2$  : 1.012

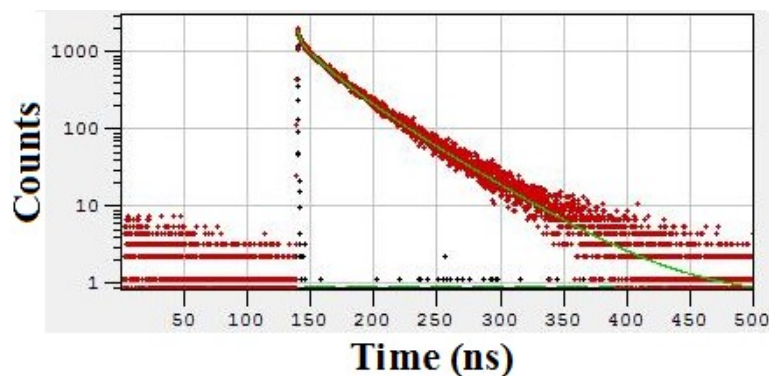
B <sub>i</sub>	$\Delta B_i$	f <sub>i</sub> (%)	$\Delta f_i$ (%)	$\tau_i$ (ns)	$\Delta \tau_i$ (ns)
----------------	--------------	--------------------	------------------	---------------	----------------------

1	345.0226	18.4528	1.191	0.075	3.296	0.031
2	488.1303	22.6494	13.341	0.620	26.104	0.002
3	1138.4395	30.1089	85.468	2.261	71.705	0.0002

Shift : 0 ns ( $\pm 0$  ns)

Decay Background : 1.191 ( $\pm 0.428$ )

Figure 17S: Time resolved fluorescence emission of solid sample of **3** ( $\lambda_{\text{ex}}$ , 405 nm;  $\lambda_{\text{em}}$ , 480 nm).



#### Exponential Components Analysis (Tail Fitting)

Fitting range : [1130; 4096] channels

$\chi^2$  : 1.018

	$B_i$	$\Delta B_i$	$f_i$ (%)	$\Delta f_i$ (%)	$\tau_i$ (ns)	$\Delta \tau_i$ (ns)
1	656.2955	16.9560	3.017	0.111	2.062	0.022
2	719.9695	28.0951	33.634	1.315	20.959	0.002
3	628.1241	33.4922	63.349	3.378	45.248	0.0004

Shift : 0 ns ( $\pm 0$  ns)

Decay Background : 0.675 ( $\pm 0.106$ )

Figure 18S: Time resolved fluorescence emission of solid sample of **4** ( $\lambda_{\text{ex}}$ , 405 nm;  $\lambda_{\text{em}}$ , 480 nm).

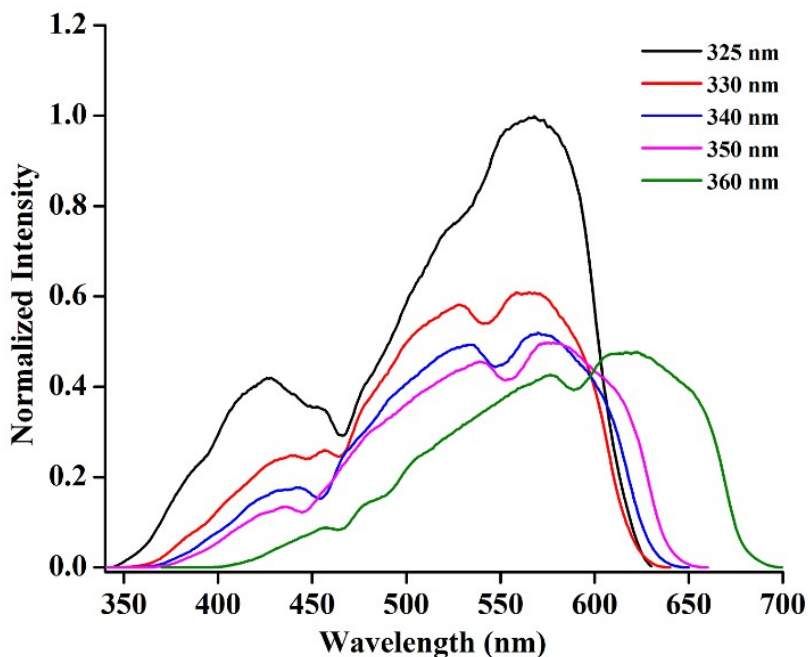


Figure 19S: Emission spectra of the solid sample of **1** upon irradiation at different wavelengths.  
(Recorded on HORIBA FLUOROMAX-4C, slit 5 nm)

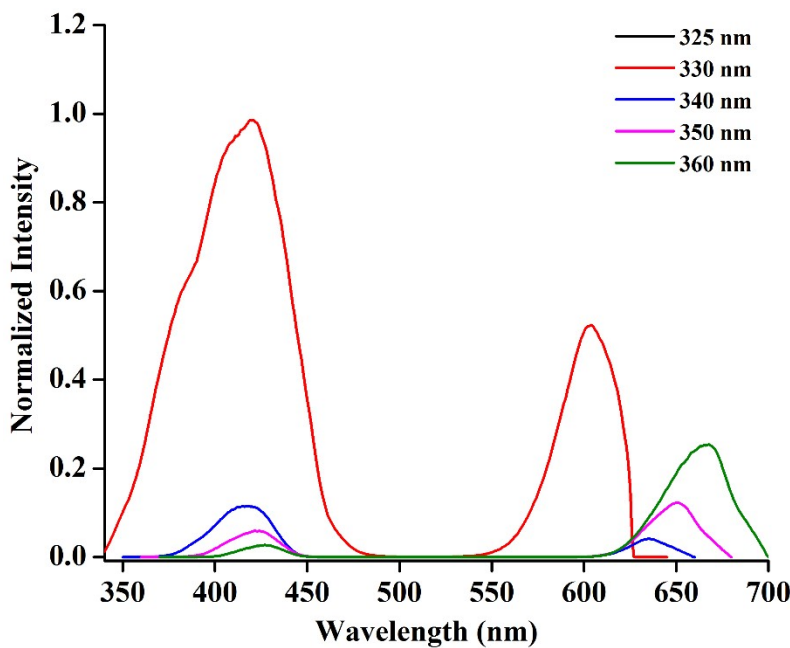


Figure 20S: Fluorescence emission spectra of the solid sample of **2** upon irradiation at different wavelengths  
(Recorded on HORIBA FLUOROMAX-4C, slit 5 nm).

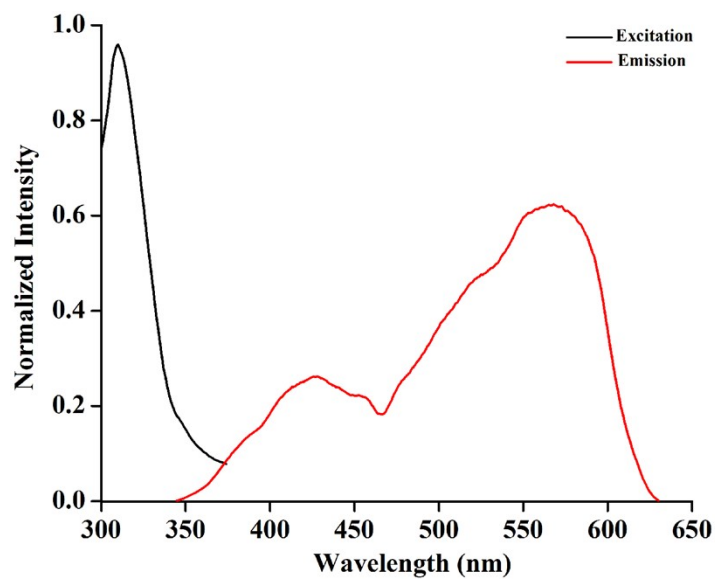


Figure 21S: Emission and excitation spectra of the solid sample of **1** upon irradiation by wavelength = 325 nm. (Recorded on HORIBA FLUOROMAX-4C, slit 5 nm)

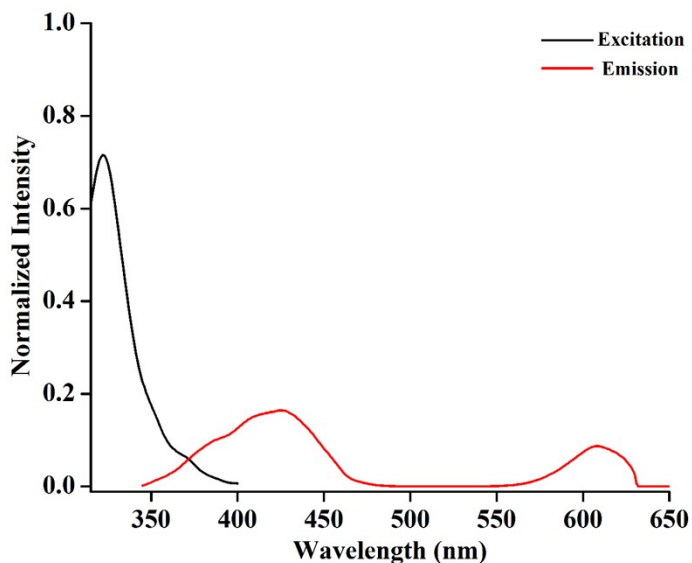


Figure 22S: Emission and excitation spectra of the solid sample of **2** upon irradiation by wavelength = 325 nm. (Recorded on HORIBA FLUOROMAX-4C, slit 5 nm)

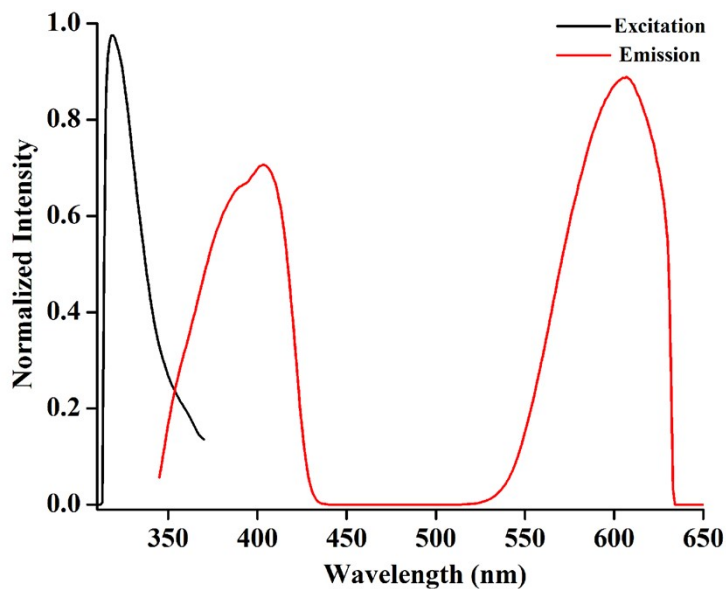


Figure 23S: Emission and excitation spectra of the solid sample of **3** upon irradiation by wavelength = 325 nm (Recorded on HORIBA FLUOROMAX-4C, slit 5 nm).

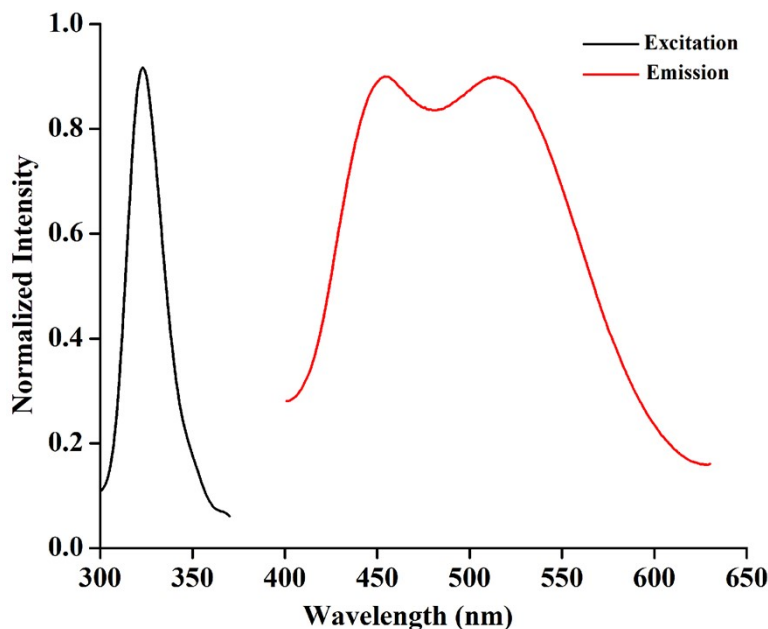


Figure 24S: Emission and excitation spectra of the solid sample of **4** upon irradiation by wavelength = 325 nm. (Recorded on HORIBA FLUOROMAX-4C, slit 5 nm)

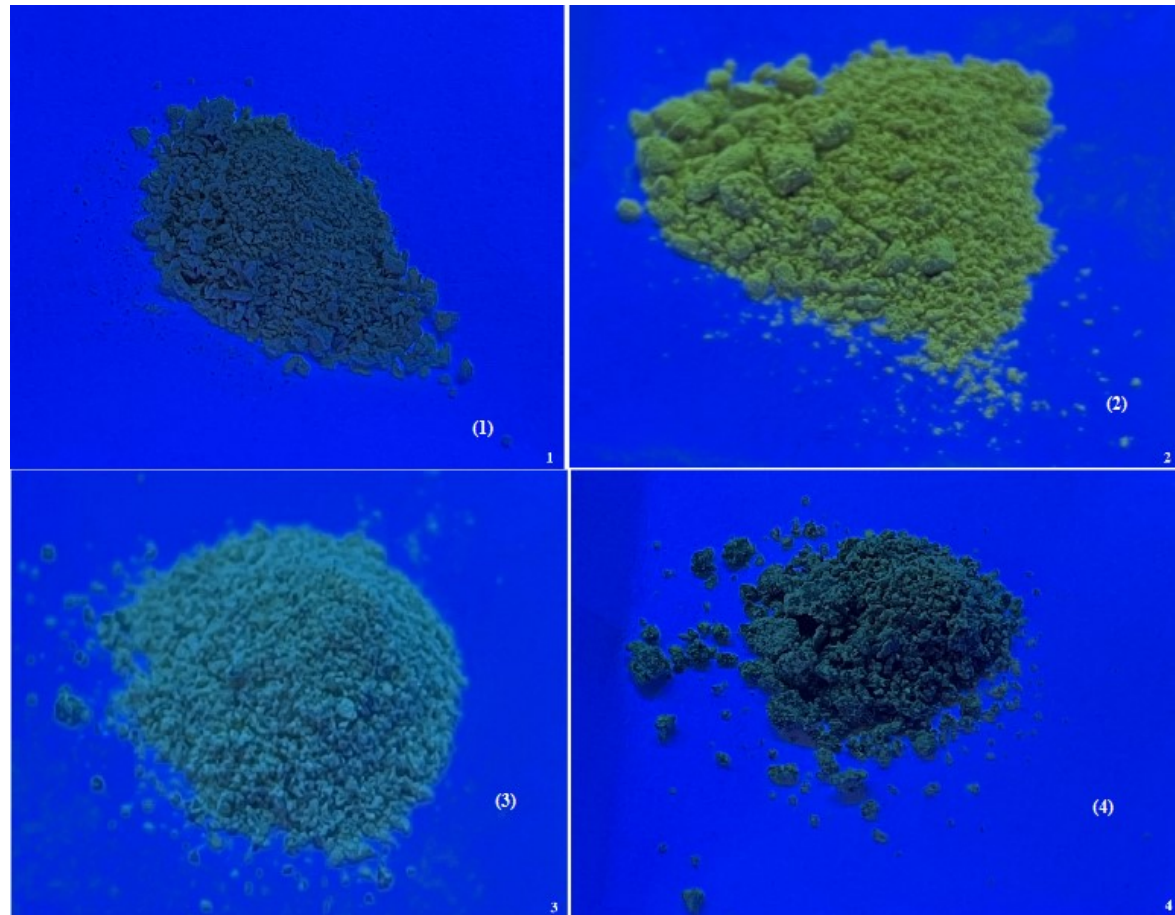


Figure 25S: The visual colour of the solid samples of 1-4 under UV-lamp

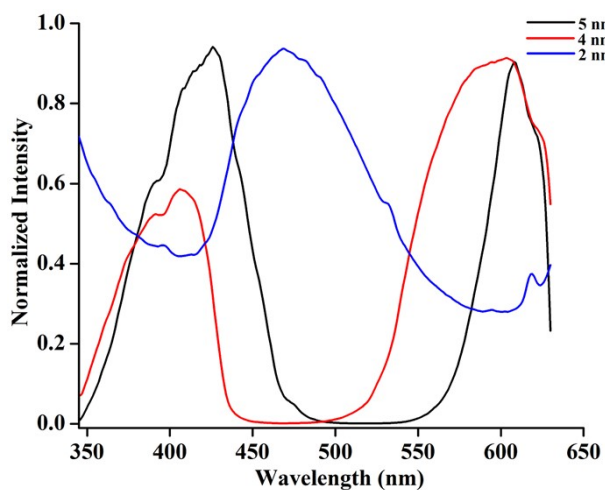


Figure 26S: Solid-state photoluminescence of the compound **2** at different slit widths (band pass black =5 nm, red = 4 nm and Blue = 2 nm) irradiation by wavelength = 325nm. (Recorded on a HORIBA FLUOROMAX-4P; Serial No. 0644D-2510-FM).

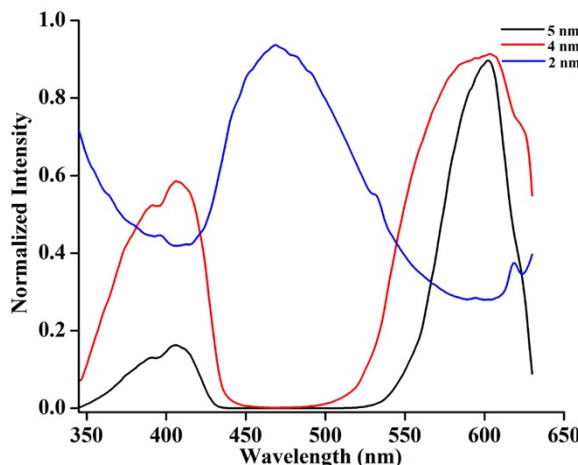


Figure 27S: Solid-state photoluminescence of the compound **3** at different slit widths (band pass black =5 nm, red = 4 nm and Blue = 2 nm) upon irradiation by wavelength = 325nm. (Recorded on a HORIBA FLUOROMAX-4P; Serial No. 0644D-2510-FM).

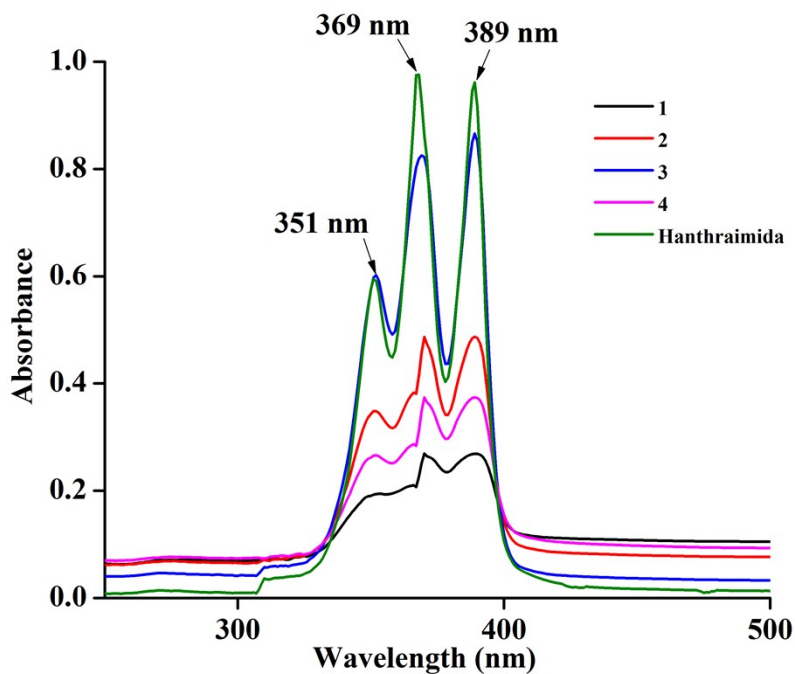


Figure 28S: UV-vis spectra of the cocrystals **1**, **2**, **3**, **4** and **Hanthraimida** ( $10^{-6}$  M in DMSO).

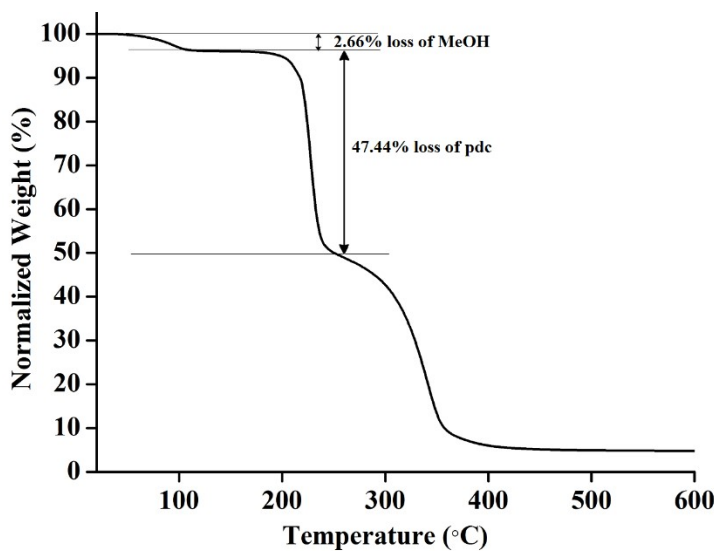


Figure 29S: Thermogravimetry of the cocrystal **1** (heating rate  $10^{\circ}\text{C}$  /minute). Theoretical value of loss of one MeOH molecule is 2.40% and experimental value is 2.66%. Theoretical value of loss of four pdc molecules is 49.87% and experimental value is 47.44%.

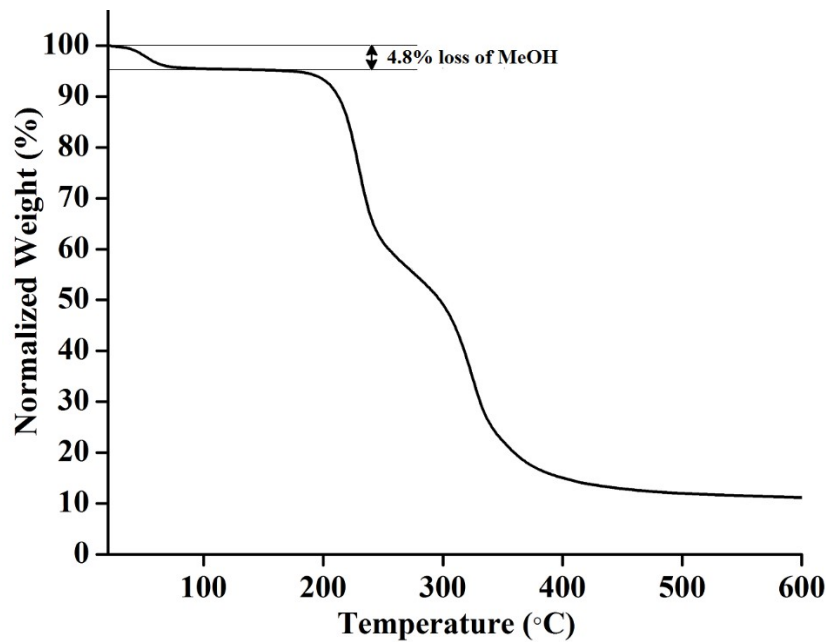


Figure 30S: Thermogravimetry of the cocrystal **3** (heating rate 10°C /minute). Theoretical value of loss of one MeOH molecule is 4.97% and experimental value is 4.8%.

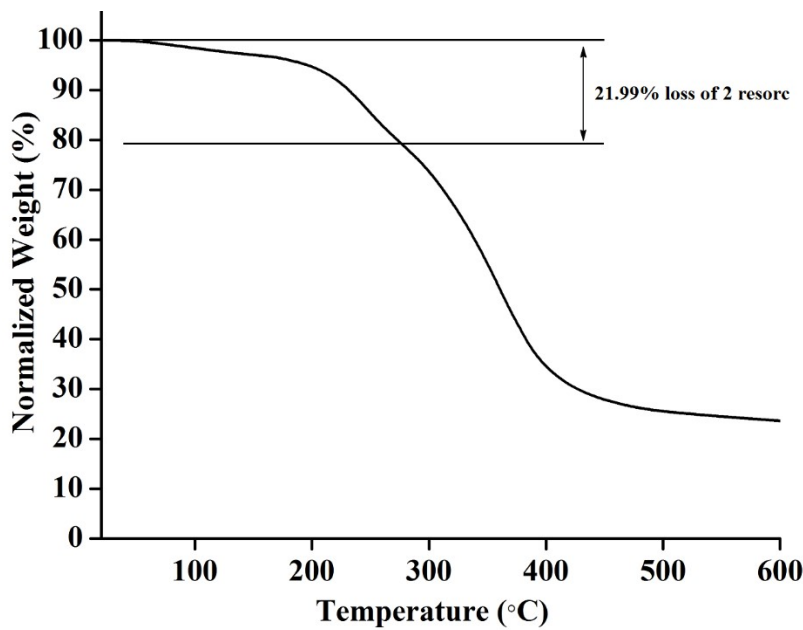


Figure 31S: Thermogravimetry of the cocrystal **1** (heating rate 10°C /minute). Theoretical value of loss of two resorc molecule is 21.6% and experimental value is 21.99%.

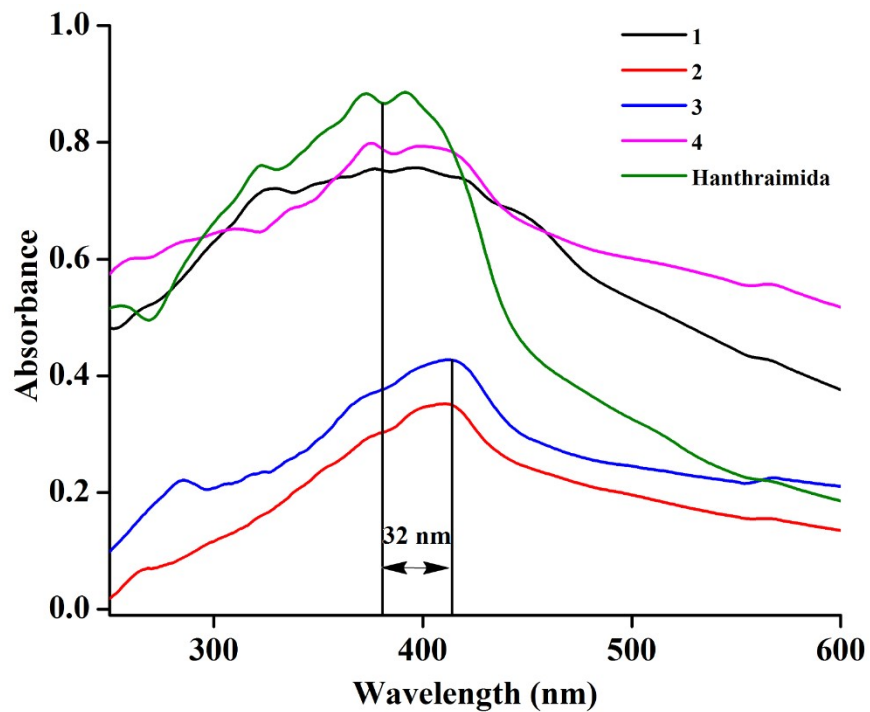


Figure 32S: Solid state UV-visible spectra of the cocrystals/salt 1-4.